

Image Reconstruction from Ipswich Data—III

P. M. van den Berg¹, B. J. Kooij¹, and R. E. Kleinman²

¹Laboratory of Electromagnetic Research
Centre for Technical Geoscience
Delft University of Technology
P. O. Box 5031
2600 GA Delft, The Netherlands
Tel: +31 15-2786254
Fax: +31 15-2786194
E-mail: p.m.vdberg@et.tudelft.nl

²Deceased; formerly with Center for the Mathematics of Waves
Department of Mathematical Sciences
University of Delaware
Newark, DE 19716 USA

Keywords: Electromagnetic scattering inverse problems, electromagnetic imaging, image reconstruction, contrast source inversion

1. Introduction

In this paper, we describe results obtained in image reconstruction using the Ipswich data sets IPS009-IPS012. In earlier work, we employed versions of the Modified Gradient Method [1-3] to reconstruct the shape, location, and index of refraction of known and unknown scatterers, both dielectric and perfectly conducting, from the measured scattered field data contained in IPS001-IPS008. In the present paper, we employ a new inversion method, the Contrast Source Inversion (CSI) Method, for the reconstructions. We include here a brief description of the method, given in greater detail in [4]. In the case of the new Ipswich experiments, we have 36 angles of incidence, equidistantly distributed around the object. The unknown scatterer is assumed to be located somewhere in a known, bounded, test domain D (taken to be square), and the scattered field is measured on a domain S (taken to be a circle) containing the test domain D in its interior. In the case of the Ipswich experiments, S was taken to be in the far zone of the scattered field, and measurements were made at 18 angles of observation, equidistantly distributed over a semicircle. For each experiment, this semicircle started with the forward-scattering angle.

2. The CSI method

Denote by \mathbf{p} and \mathbf{q} position vectors in \mathbb{R}^2 , and let B denote a bounded, not-necessarily-connected, scattering object (or objects). The exact location and index of refraction or contrast of the scattering object is unknown, but it is known to lie within another, larger, bounded simply connected domain, D . If $u_j^{inc}(\mathbf{p}) = u_j^{inc}(\mathbf{p}, \mathbf{q}_j)$ denotes an incident wave with wavenumber k (assumed to be real) and source point \mathbf{q}_j (\mathbf{q}_j is replaced by the unit vector $\hat{\mathbf{q}}_j$ for plane waves), then for a large class of scattering problems, the total field in D is known to satisfy the integral equation

$$u_j(\mathbf{p}) = u_j^{inc}(\mathbf{p}) + k^2 \int_D G(\mathbf{p}, \mathbf{q}) \chi(\mathbf{q}) u_j(\mathbf{q}) dv(\mathbf{q}), \quad (1)$$

where $G(\mathbf{p}, \mathbf{q})$ denotes the Green's function of the background medium:

$$G(\mathbf{p}, \mathbf{q}) = \frac{i}{4} H_0^{(1)}(k|\mathbf{p} - \mathbf{q}|). \quad (2)$$

χ denotes the complex contrast:

$$\chi(\mathbf{q}) = \chi^r(\mathbf{q}) + i\chi^i(\mathbf{q}) = \frac{\varepsilon(\mathbf{q}) - \varepsilon_0}{\varepsilon_0} + i \frac{\sigma(\mathbf{q})}{\omega\varepsilon_0}, \quad (3)$$

where ε_0 and μ_0 are the permittivity and the permeability of the (lossless) background, while $\varepsilon(\mathbf{q})$ and $\sigma(\mathbf{q})$ are the permittivity and conductivity of the scatterer, which is assumed to be nonmagnetic. Observe that if \mathbf{p} is not in B , then χ vanishes; but if the location of B is unknown, then it is not known a priori where χ vanishes. However, with the assumption that $B \subset D$, it is known that χ vanishes for \mathbf{p} outside D . In fact, denoting by S a domain (or curve, or a discrete collection of points) outside of D where the scattered field is measured to be $f_j(\mathbf{p})$, Equation (1) becomes

$$f_j(\mathbf{p}) = k^2 \int_D G(\mathbf{p}, \mathbf{q}) \chi(\mathbf{q}) u_j(\mathbf{q}) dv(\mathbf{q}), \quad \mathbf{p} \in S, \quad (4)$$

if there is no noise or error in the measurements. But error-free data are extremely unlikely, and we do not assume that Equation (4) holds exactly. Rewriting Equations (1) and (4) in symbolic form, we have the object or state equations

$$u_j = u_j^{inc} + G_D \chi \mu_j, \quad \mathbf{p} \in D, \quad (6)$$

and the data equations

$$f_j = G_S \chi \mu_j, \quad \mathbf{p} \in S. \quad (7)$$

The subscripts D and S on the operators defined implicitly in Equations (1) and (4) are added to accentuate the location of the point \mathbf{p} , since the operators are identical in all other respects.

In the absence of other a priori information, Equations (5) and (6) are the only equations we have relating the unknown contrast χ (which, recall, consists of at most two unknown real-valued functions), and the unknown fields, u_j , in D . The known data consist of the incident fields, u_j^{inc} , the measured data, f_j , and the test domain, D . Because the contrast and fields occur as a product, we introduce the contrast sources

$$w_j = \chi u_j. \quad (7)$$

Then, the data equations become

$$f_j = G_S w_j, \quad (8)$$

while the state equations become

$$u_j = u_j^{inc} + G_D w_j, \quad (9)$$

or, with Equation (7),

$$\chi u_j^{inc} = w_j - \chi G_D w_j. \quad (10)$$

Following a similar procedure to that used in the Modified Gradient Method [1-3], we now simultaneously construct sequences of sources $w_{j,n}$ and contrasts χ_n that converge to minima of the cost functional,

$$F = \frac{\sum_j \|f_j - G_S w_j\|_S^2}{\sum_j \|f_j\|_S^2} + \frac{\sum_j \|\chi u_j^{inc} - w_j + \chi G_D w_j\|_D^2}{\sum_j \|\chi u_j^{inc}\|_D^2}, \quad (11)$$

where $\|\cdot\|_S^2$ and $\|\cdot\|_D^2$ denote the norms on $L_2(S)$ and $L_2(D)$, respectively. The normalization is chosen so that both terms are equal to one if $w_j = 0$. The first term measures the error in the data equations, and the second term measures the error in the form of the state equations given in Equation (10). This is a quadratic functional in w_j , but highly nonlinear in χ . We propose an iterative minimization of this cost functional, using an alternating method that first updates w_j and then updates χ . Thus, we construct sequences $\{w_{j,n}\}$ and $\{\chi_n\}$, for $n=0, 1, 2, \dots$, in the following manner.

Define the data error to be

$$\rho_{j,n} = f_j - G_S w_{j,n}, \quad (12)$$

and the state error to be

$$r_{j,n} = \chi_n u_{j,n} - w_{j,n}, \quad (13)$$

where

$$u_{j,n} = u_j^{inc} + G_D w_{j,n}. \quad (14)$$

Now suppose $w_{j,n-1}$ and χ_{n-1} are known. We update w_j by

$$w_{j,n} = w_{j,n-1} + \alpha_n v_{j,n}, \quad (15)$$

where α_n is constant, and the update directions, $v_{j,n}$, are functions of position.

The update directions are chosen to be the Polak-Ribière conjugate-gradient directions:

$$v_{j,0} = 0, \\ v_{j,n} = g_{j,n} + \frac{\sum_k \langle g_{k,n}, g_{k,n} - g_{k,n-1} \rangle_D}{\sum_k \langle g_{k,n-1}, g_{k,n-1} \rangle_D} v_{j,n-1}, \quad n \geq 1, \quad (16)$$

where $g_{j,n}$ is the gradient (Fréchet derivative) of the cost functional with respect to w_j , evaluated at $w_{j,n-1}, \chi_{n-1}$, while $\langle \cdot, \cdot \rangle_D$ denotes the inner product on $L_2(D)$. Explicitly, this is found to be

$$g_{j,n} = -\frac{G_S^* \rho_{j,n-1}}{\sum_k \|f_k\|_S^2} - \frac{r_{j,n-1} - G_D^* (\bar{\chi}_{n-1} r_{j,n-1})}{\sum_k \|\chi_{n-1} u_k^{inc}\|_D^2}, \quad (17)$$

where G_S^* and G_D^* are the adjoints of G_S and G_D mapping $L_2(S)$ into $L_2(D)$ and $L_2(D)$ into $L_2(D)$, respectively. Furthermore, the over-bar denotes complex conjugate.

With the update directions completely specified, the constant α_n is determined to minimize the cost functional Equation (11), and is found explicitly to be

$$\alpha_n = \frac{\frac{\sum_j \langle \rho_{j,n-1}, G_S v_{j,n} \rangle_S + \sum_j \langle r_{j,n-1}, v_{j,n} - \chi_{n-1} G_D v_{j,n} \rangle_D}{\sum_j \|f_j\|_S^2}}{\frac{\sum_j \|G_S v_{j,n}\|_S^2 + \sum_j \|v_{j,n} - \chi_{n-1} G_D v_{j,n}\|_D^2}{\sum_j \|f_j\|_S^2 + \sum_j \|\chi_{n-1} u_j^{inc}\|_D^2}}, \quad (18)$$

where $\langle \cdot, \cdot \rangle_S$ denotes the inner product on $L_2(S)$.

Once $w_{j,n}$ is determined, $u_{j,n}$ is obtained via Equations (14) and (15) as

$$u_{j,n} = u_j^{inc} + G_D v_{j,n}. \quad (19)$$

We then seek χ to minimize the cost functional

$$F'_D = \sum_j \|\chi u_{j,n} - w_{j,n}\|_D^2. \quad (20)$$

We now have a priori information that χ^r and χ^i are positive. This leads to

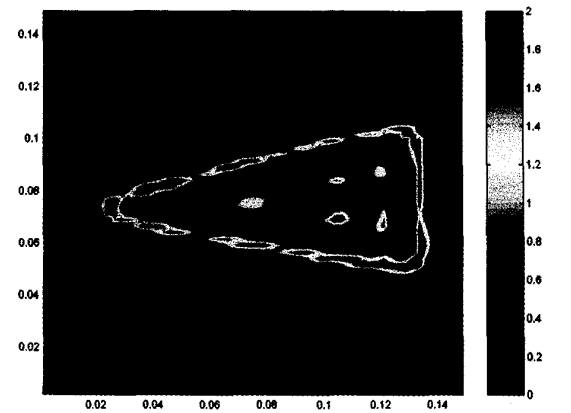
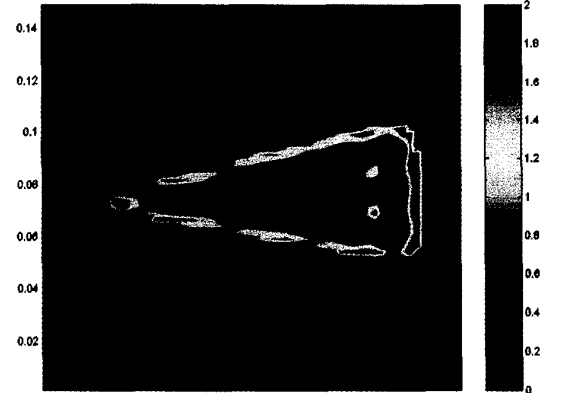
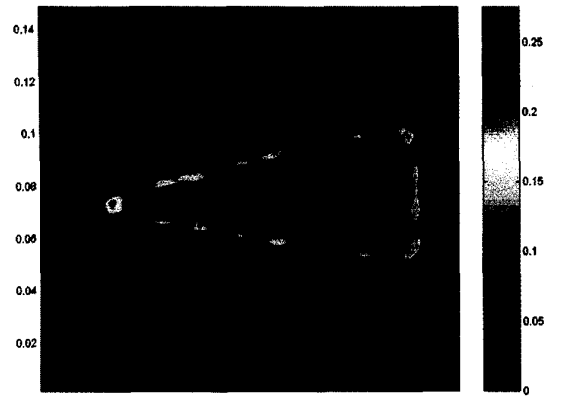
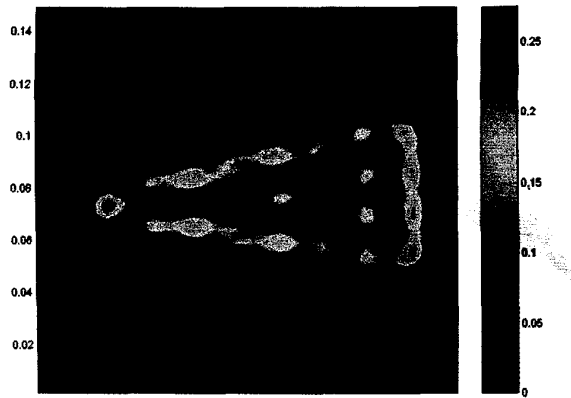


Figure 1. Reconstruction of the triangular aluminum object IPS009: a) χ_0^r ; b) χ_0^i ; c) χ_{128}^r ; d) χ_{128}^i .

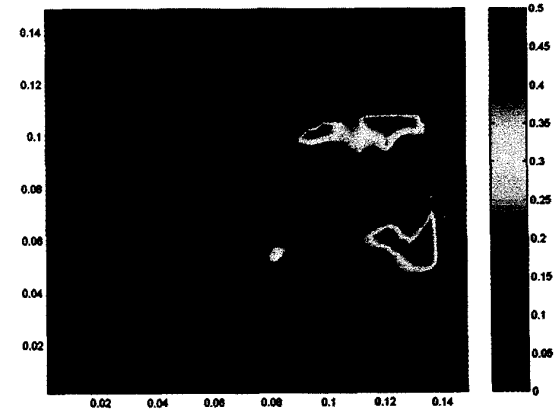
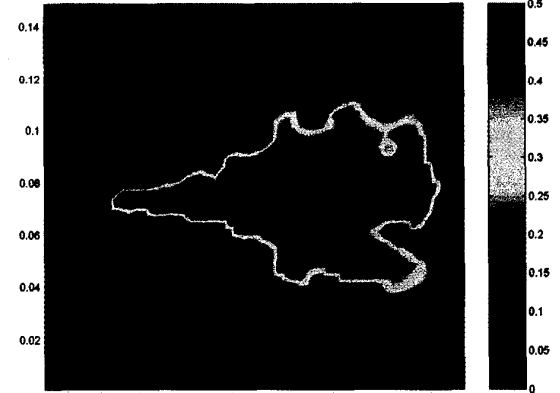
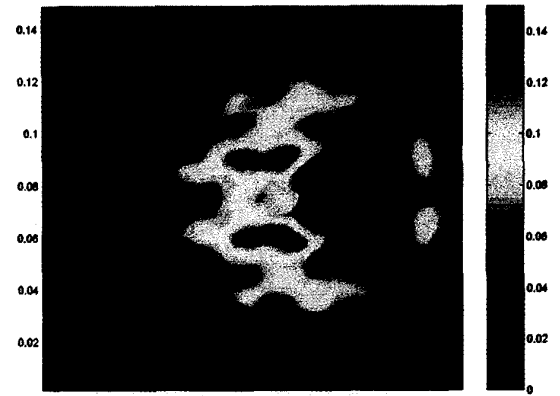
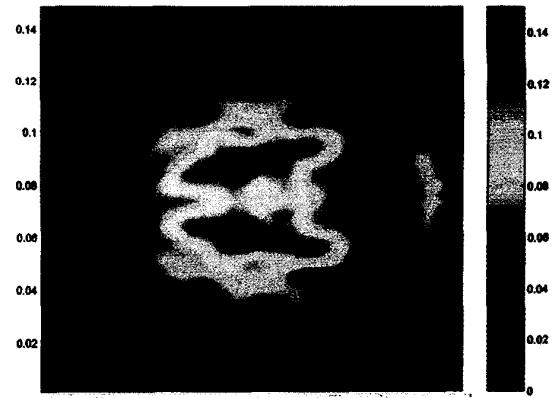


Figure 2. Reconstruction of the mystery penetrable object IPS010: a) χ_0^r ; b) χ_0^i ; c) χ_{512}^r ; d) χ_{512}^i .

$$\chi_n^r = \left\{ \frac{\sum_j \left[\frac{\text{Re}(w_{j,n} \bar{u}_{j,n})}{|u_{j,n}|} \right]^2}{\sum_j |u_{j,n}|^2} \right\}^{1/2}, \quad (21)$$

$$\chi_n^i = \left\{ \frac{\sum_j \left[\frac{\text{Im}(w_{j,n} \bar{u}_{j,n})}{|u_{j,n}|} \right]^2}{\sum_j |u_{j,n}|^2} \right\}^{1/2}.$$

This completes the description of the algorithm, except for designating the starting values, $w_{j,0}$. Observe that we cannot start with $w_{j,0} = 0$, since then $\chi_0^r = \chi_0^i = 0$, and the cost functional, Equation (11), is undefined. Therefore, we choose as starting values the values obtained by back-propagation:

$$w_{j,0}^{bp} = - \frac{\|G_S^* f_j\|_D^2}{\|G_S G_S^* f_j\|_S^2} G_S^* f_j. \quad (22)$$

This completes the description of the algorithm.

3. Calibration of the Ipswich data sets

One of the persistent problems in using the Ipswich data sets concerns the phase of the measured data. Since the measurements provide relative phase only, some means is needed to normalize the data, so that it coincides in phase with the actual scattered field. That there is a phase shift became evident with the 1997 Ipswich data. It was found that, using the calibration described in [3], the contrast converged to zero, with a resultant 100% error in the cost functional. The following alteration in the algorithm was made, which provides a phase correction without any additional information about the experiments. We iteratively update the data f_j as follows:

$$f_{j,0} = f_j, \quad f_{j,n} = \frac{c_n}{|c_n|} f_{j,n-1}, \quad (23)$$

where c_n is a complex constant, and is found by minimizing the data error $\sum_j \|c_n f_{j,n-1} - G_S w_{j,n}\|_S^2$. Then, we define a new data error as

$$\bar{\rho}_{j,n} = f_{j,n} - G_S w_{j,n}. \quad (24)$$

The algorithm given above is changed only by using $\bar{\rho}_{j,n-1}$ and $f_{j,n-1}$ in place of $\rho_{j,n-1}$ and f_j in Equations (17) and (18). Clearly, after n iterations, we have

$$f_{j,n} = C_n f_j, \quad C_n = \prod_{m=1}^n \frac{c_m}{|c_m|}. \quad (25)$$

Interestingly, when this modification was used on the 1996 data

sets, we found that $C_n \rightarrow 1$ for increasing n , whereas for the 1997 data sets, $C_n \rightarrow -1$ for increasing n . This once again indicates the fact that data sets presented in a non-uniform manner can present serious problems for inversion algorithms that depend on phase information. However, the technique described here can alleviate this problem.

4. IPS009

We first present the reconstructed images using the Ipswich data set, IPS009, which was known to be a triangular aluminum object with additional a priori information that the object was located inside a circle of radius of 6 cm. We took a test domain, D , with sides of 15 cm, or 5λ (since the wavelength, λ , in all experiments was 3 cm). The test domain was subdivided into 60×60 sub-squares for the computations. Figure 1 depicts the reconstruction results. Figures 1a and 1b are respectively the real and imaginary parts of the contrast, χ_0^r and χ_0^i , after the initial step (back-propagation using reciprocity [3]). Figures 1c and 1d show the real and imaginary parts of the contrast, χ_{128}^r and χ_{128}^i , after 128 iterations. After 128 iterations, the image did not improve significantly, although the contrast at the boundary of the object did increase with additional iterations. This phenomenon indicates that the scatterer was impenetrable. The triangular shape is very visible. Inside the object, the reconstructed contrast has no meaning at all, since the interior fields for an impenetrable object are undefined. Note that the color scale covers a much smaller range for the initial reconstruction, in order to magnify the image.

5. IPS010

We now consider the first mystery object, with a priori information that the object is penetrable and lies inside a circle of radius of 6 cm. We took the same test domain, D , as in the previous example. The reconstruction results are depicted in Figure 2. Figures 2a and 2b are the real and imaginary parts of the contrast, χ_0^r and χ_0^i , after the initial step (back-propagation using reciprocity). Figures 2c and 2d are the real and imaginary parts of the contrast, χ_{512}^r and χ_{512}^i , after 512 iterations. After 512 iterations, the image did not improve significantly. From this image, a triangular shape is very visible, and the major part of the contrast is real valued. Hence, we guessed that this mystery object was a triangular object with a real permittivity, $\epsilon/\epsilon_0 \approx 1.5$. The dimensions can be guessed from the bottom images. Figure 1d indicates that the object also has a non-zero imaginary contrast (a conductive part). But closer observation shows that the imaginary contrast fits in the indentations at the right side of the real contrast. This indicates that the data, for illuminations at the right side of the object, may have some substantial phase discrepancies. Again, note that the color scales cover different intensity ranges in the two reconstructions, although the difference is not as great as for IPS009.

6. IPS011

In this example, we have a priori information that the object is an aluminum circular cavity, and lies inside a circle of radius of 6 cm. We took the same test domain, D , as in the previous

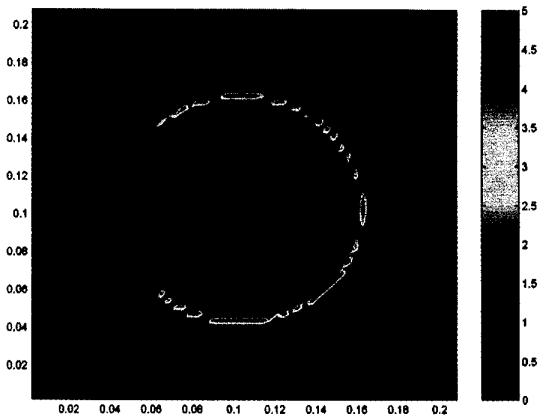
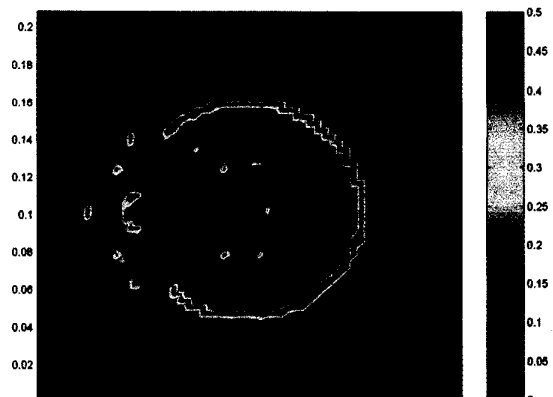
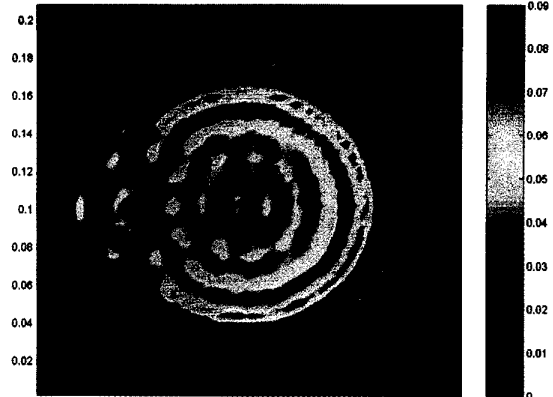
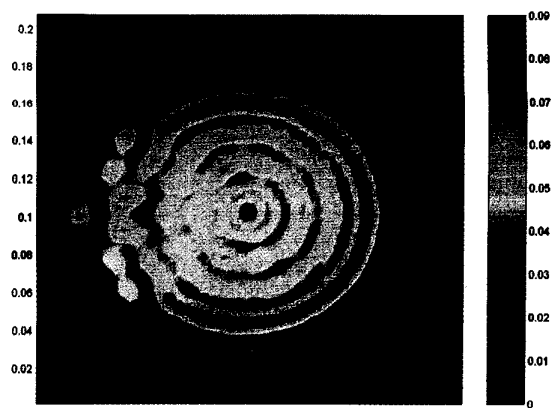
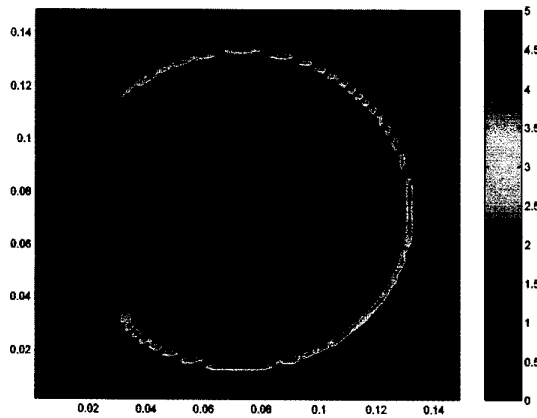
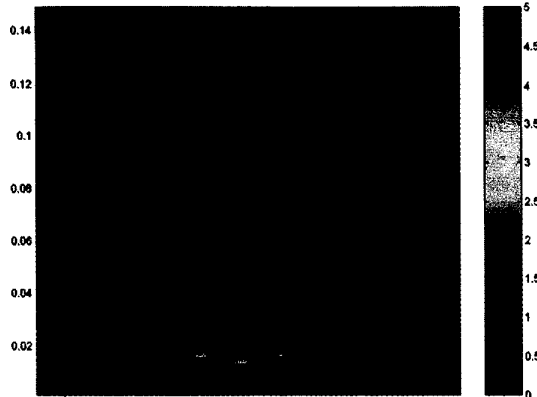
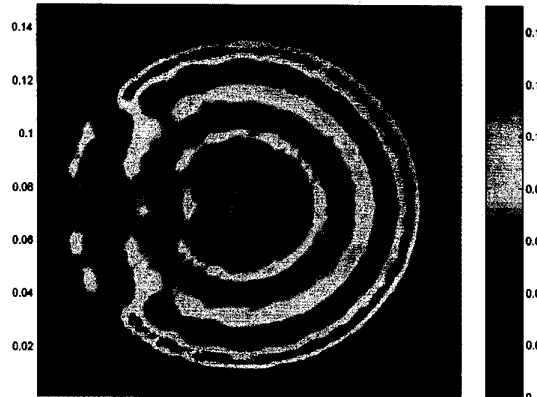
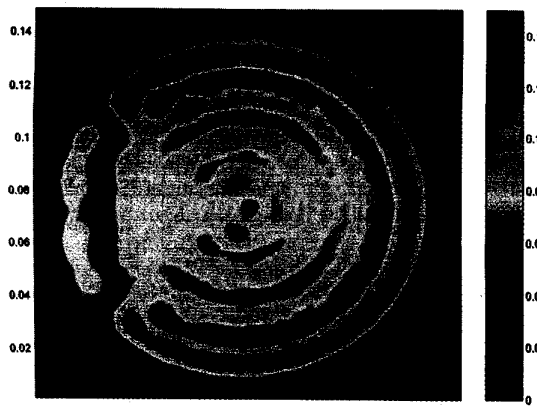


Figure 3. Reconstruction of the aluminum circular cavity (IPS011): a) χ_0^i ; b) χ_0^f ; c) χ_{128}^i ; d) χ_{128}^f .

Figure 4. Reconstruction of the mystery hybrid object (IPS012): a) χ_0^i ; b) χ_0^f ; c) χ_{512}^i ; d) χ_{512}^f .

examples. The reconstruction results are depicted in Figure 3. Figures 3a and 3b show the real and imaginary parts of the contrast, χ_0^r and χ_0^i , after the initial step (back-propagation using reciprocity). Figures 3c and 3d show the real and imaginary parts of the contrast, χ_{128}^r and χ_{128}^i , after 128 iterations. After 128 iterations, the image did not improve significantly, although the contrast at the boundary of the object increased further with an increasing number of iterations, which indicates, as with IPS009, that the scatterer is impenetrable. The image clearly shows that the object is an open circular shell. The very small thickness of the shell is reconstructed very well. At the edges on the left side there is some distortion, probably due to the edge behavior of the fields and contrast sources. There is also some distortion present inside the cavity, but that can be understood if one takes into account that the major part of the interior of the cavity is shielded from all but a few of the sources and receivers. Here, again, observe the magnification of the color scale for the initial reconstruction, which was needed to make the image visible.

7. IPS012

We now consider the second mystery object, where we have a priori information that the object is hybrid, partly penetrable and partly impenetrable, and, moreover, lies inside a circle of radius of 9 cm. We took a test domain, D , with sides of 21 cm, or 7λ . The test domain was again subdivided into 60×60 sub-squares for the computations. The reconstruction results are depicted in Figure 4. Figures 4a and 4b show the real and imaginary parts of the contrast, χ_0^r and χ_0^i , after the initial step (back-propagation using reciprocity). Figures 4c and 4d show the real and imaginary parts of the contrast, χ_{512}^r and χ_{512}^i , after 512 iterations. We chose this number of iterations because in the case of IPS010, the penetrable object, we needed to take this large number of iterations to reconstruct the real part of the contrast, and we reasoned that we would again need this number to reconstruct the real part of the contrast, which would give information about the penetrable part of the object. The image clearly shows that the impenetrable part of the object is an open circular (impenetrable) shell. It is obvious that this shell is the aluminum shell of the previous example. The very

small thickness of the shell is again reconstructed very well. From the real part of the contrast, we observe that there is a penetrable object present, both inside and outside the cavity. With some imagination, one can surmise that inside the aluminum shell of IPS011, the triangular penetrable object of IPS010 has been positioned; but, again, it is noted that reconstructions of objects inside the cavity can hardly be reconstructed with the present data set, because the major part of the interior domain of the cavity is shielded, and only sources and receivers at the left side of the object can illuminate and probe this interior domain. Note, also, that the magnitude of the color scale of Figure 4c differs from that for Figure 4d, which was needed to observe the penetrable parts of the object.

8. Acknowledgements

This work was supported by the Technology Foundation (STW), the Netherlands, and by the Air Force Office of Scientific Research, Air force Material Command, USAF, under Grant F9620-96-1-0039.

9. References

1. P. M. van den Berg, G. Coté, and R. E. Kleinman, "Blind' Shape Reconstruction from Experimental Data," *IEEE Transactions on Antennas and Propagation*, **AP-43**, 1995, pp. 1389-1396.
2. P. M. van den Berg and R. E. Kleinman, "Image Reconstruction from Ipswich Data," *IEEE Antennas and Propagation Magazine*, **38**, 1996, pp. 56-59.
3. P. M. van den Berg, B. J. Kooij, and R. E. Kleinman, "Image Reconstruction from Ipswich Data-II," *IEEE Antennas and Propagation Magazine*, **39**, 1997, pp. 29-32.
4. P. M. van den Berg and R. E. Kleinman, "A Contrast Source Inversion Method," *Inverse Problems*, **13**, 1997, to be published.